

# Structure of Classifier Boundaries: Case Study for a Naïve Bayes Classifier

Alan F. Karr\*, Zac Bowen†, Adam A. Porter‡

December 9, 2022

## Abstract

Whether based on models, training data or a combination, classifiers place (possibly complex) input data into one of a relatively small number of output categories. In this paper, we study the structure of the *boundary*—those points for which a neighbor is classified differently—in the context of an input space that is a graph, so that there is a concept of neighboring inputs. The scientific setting is a model-based naïve Bayes classifier for DNA reads produced by Next Generation Sequencers (NGSs). We show that the boundary is both large and complicated in structure. We create a new measure of uncertainty, called Neighbor Similarity, that compares the result for a point to the distribution of results for its neighbors. This measure not only tracks two inherent uncertainty measures for the Bayes classifier, but also can be implemented, at a computational cost, for classifiers without inherent measures of uncertainty.

**Key words:** classifier, Bayes classifier, uncertainty, metagenomics, DNA reads

## 1 Introduction

In today’s world, classifiers are ubiquitous. They are used in facial recognition, for military purposes, by autonomous vehicles, and—to the point of this paper, assembly of DNA reads in metagenomics. Inputs include numerical data, character strings, images and sound clips. The underlying statistical methodologies range from maximum likelihood for mixture models to Bayes methods (as in this paper) to neural networks and deep learning based on labeled “training data.” Classifiers may or (more often, it seems) may not produce even informal measures of confidence, let alone quantified measures of uncertainty.

Typically, the input space for a classifier is both high-dimensional and enormous, while the output space is much smaller. For instance, in our experiment (Section 2), the input space has cardinality  $5^{101}$ , and the output space has cardinality 3. When the input space is a graph, which in our case study and many other contexts it is, much insight can be gained from understanding the *classifier boundary*, which is comprised of those points with one or more neighbors that are classified differently. From the input data perspective, these points are fragile, because changing them ever so slightly changes the output dramatically. And as we show below, quantifying this difference yields a surrogate measure of uncertainty that is computable for any classifier whose input space is a graph.

---

\*Fraunhofer USA Center Mid-Atlantic and Temple University, Department of Statistics, Operations, and Data Science; akarr@fraunhofer.org; Corresponding author

†Fraunhofer USA Center Mid-Atlantic; zbowen@fraunhofer.org

‡University of Maryland, Department of Computer Science, and Fraunhofer USA Center Mid-Atlantic; aporter@cs.umd.edu

From the classifier perspective, understanding the boundary illuminates how the classifier works. Is the boundary large or small? Is its geometry simple or complex? How can it best be studied? For our case study, the boundary in no way resembles boundaries for smooth functions, i.e., level sets. It is, by contrast,

**Large;** possibly as large as 20% of the input space, and not of lower dimension;

**Complex geometrically,** and possibly fractal-like in nature; and

**Explorable** in multiple ways.

The remainder of this paper is organized in the following manner. In Section 2 we describe our experiment: the scientific setting, the data and the Bayes classifier, as well as introduce two surrogate uncertainty measures. Section 3 contains results for the DNA reads, together with techniques for exploring the boundary. Sections 4 and 5 contain discussion and conclusions, respectively.

## 2 Experimental Setting

In this paper, a DNA sequence  $G$  is a character string chosen from the nucleotide (base) alphabet  $\mathcal{N} = \{A, C, G, T\}$ . At one extreme,  $G$  may be an entire genome—for instance, a virus or a chromosome. At another, it may be a simulated read generated by a NGS, in our case, an Illumina sequencer. Given a sequence  $G$ , the length of  $G$  is  $|G|$ ; the  $i^{\text{th}}$  base in  $G$  is  $G(i)$ ; and the bases from location  $i$  to location  $j > i$  are  $G(i : j)$ . For  $k \geq 1$ , let  $\mathcal{N}(k)$  be the set of all sequences of length  $k$  from  $\mathcal{N}$ , of which there are  $4^k$ . As in (Karr et al., 2022a), we focus on triplets, whose distributions are 64-dimensional summaries of sequences. Other cases appear in the literature, especially quartets, which are also referred to as tetranucleotides (Pride et al., 2003; Teeling et al., 2004a,b).

### 2.1 Preliminaries

Here, a classifier is a function  $C$  from a finite input space  $\mathcal{I}$  to a finite output space  $\mathcal{O}$ . Elements of  $\mathcal{I}$  are termed *inputs* or *data*, and  $C(x) \in \mathcal{O}$  is the *decision* or *result* for input  $x$ . Elements of  $\mathcal{O}$  are sometimes also termed categories or classes. Although it is not a logical necessity, there is little point in constructing or using a classifier unless  $|\mathcal{I}| \gg |\mathcal{O}|$ , where  $|S|$  is the cardinality of the set  $S$ . As noted, in our case study, 101 nucleotides with 5 possible values each (see Section 2.3) yield  $|\mathcal{I}| = 5^{101}$ , and three genomes yield  $|\mathcal{O}| = 3$ .

Although also not a necessity, we restrict attention to classifiers that are deterministic: for an input  $x$ , there is a unique, reproducible output  $C(x)$ . In our case study,  $C$  is based on maximizing Bayesian posterior probabilities, which has the advantage that there is an inherent measure of uncertainty to which the surrogate measures proposed in Section 2.6 can be compared. Mixture models that represent the effects of (discrete) latent variables are of the same ilk (Titterton et al., 1985). By contrast, deep learning and neural network models use a set  $\mathcal{T} = \{t_1, \dots, t_m\} \subseteq \mathcal{I}$  of labeled training data to set numerical parameters of  $C$  in such a way that  $C(t_j)$  is equal to a known value  $D_j$  for each  $j$ .

We further assume that the input space  $\mathcal{I}$  is an *loopless, undirected graph*: there is subset  $N$  of  $\mathcal{I} \times \mathcal{I}$  such that:

- $(x, y) \in N$  if and only if  $(y, x) \in N$ ;

- $(x, x) \notin N$  for all  $x$ .

We say that  $x, y \in \mathcal{I}$  are *neighbors* if  $(x, y) \in N$ , we denote by  $N(x) = \{y : (x, y) \in N\}$  the set of neighbors, or neighborhood, of  $x$ . For ease of interpretation and because it is true in our case study, we further assume that  $\mathcal{I}$  is *connected* graph: for any  $x, y \in \mathcal{I}$ , there is a path  $(x_1 = x, \dots, x_k = y)$  that connects them:  $(x_j, x_{j+1}) \in N$  for each  $j$ .

To illustrate in an alternative context, for image classification,  $\mathcal{I}$  may consist of all  $512 \times 512$  images with RGB values in  $\{0, \dots, 255\}$ , with  $(x = (x(r), x(g), x(b)), y = (y(r), y(g), y(b))) \in N$  if and only if they differ by one in one pixel:

$$|x(r) - y(r)| + |x(g) - y(g)| + |x(b) - y(b)| = 1.$$

For this example,  $|\mathcal{I}| = (256^3)^{512 \times 512}$ , and for most elements  $x$  of  $\mathcal{I}$ ,  $|N(x)| = 1,572,864 = 512 \times 512 \times 6$ . Points on the edges of  $\mathcal{I}$ , i.e., with one or more pixel values equal to 0 or 255, have fewer neighbors. At the extreme, the images for which all pixel values are zero or all pixel values are 255 have “only”  $786,432 = 512 \times 512 \times 3$  neighbors. We will return to this illustration when discussing computational burdens.

In our case study, consists of three virus genomes that give rise to (simulated) reads produced by a Next Generation Sequencer, and has no particular structure.

## 2.2 Three Genomes

Our scientific context is metagenomic assembly—classifying and piecing together fragments (reads) of DNA from multiple but (presumed) known sources into longer sequences called contigs. We focus on one step in reference-guided assembly, namely, assigning reads to sources. Specifically, there are three reference genomes: an adenovirus genome of length 34,125, downloaded with the read simulator `Art`, which we call Adeno; a SARS-CoV-2 genome of length 29,926 contained in a coronavirus dataset downloaded from National Center for Biotechnology Information (NCBI) in November, 2020, which we call COVID; and a SARS-CoV genome of length 29,751 from the same database, which we call SARS. Thus,  $\mathcal{O} = \{\text{Adeno}, \text{COVID}, \text{SARS}\}$ .

Moving to mathematical details, the *triplet distribution*  $P_3(\cdot|G)$  of a sequence  $G$  is defined as

$$P_3(b_1 b_2 b_3 | G) = \text{Prob}\{G(k : k + 2) = b_1 b_2 b_3\} \quad (1)$$

for each choice of  $b_1 b_2 b_3$ , where  $b_1, b_2$  and  $b_3$  are elements of  $\mathcal{N} = \{A, C, G, T\}$ , and  $k$  is chosen at random from  $1, \dots, |G| - 2$ . An equivalent perspective is that of a second-order Markov chain. The information contained in  $P_3(\cdot|G)$  is the same as that contained in the pair distribution  $P_2(\cdot|G)$  and the  $16 \times 4$  transition matrix

$$T_3((b_1, b_2), b_3 | G) = \text{Prob}\{G(k + 2) = b_3 | G(k) = b_1, G(k + 1) = b_2\}, \quad (2)$$

whose rows are indexed by  $(b_1, b_2)$  and columns are indexed by  $b_3$ , and which gives the distribution of each base conditional on its two predecessors.

Table 10 in Appendix A contains the triplet distributions for these three virus genomes. Measured by Hellinger distance,<sup>1</sup> the genomes are very different. The distances are 0.234 for Adeno/COVID, 0.125 for

---

<sup>1</sup>The definition is given in (7).

Adeno/SARS and 0.161 for COVID/SARS. To gauge these differences, the empirical 0.001  $p$ -values for distributions of genomes of the same size simulated from each distribution are 0.01941755 for adenovirus, 0.02094808 for COVID, and 0.02065539 for SARS.

### 2.3 DNA Read Data

The read dataset is the same as in Karr et al. (2022a). We employed the `Mason_simulator` read simulator (Holtgrewe, 2010) to simulate Illumina<sup>2</sup> NGS reads of length 101 from each genome, with approximate 6X coverage. The numbers of reads are 1966, 1996 and 1907, respectively; the total number of reads is 5869. The `Mason_simulator` introduces errors in the form of transpositions (single nucleotide polymorphisms (SNPs)), insertions, deletions and undetermined bases.<sup>3</sup> The latter, following convention, appear in the simulated reads as “N” and must be accommodated in computation of likelihood functions (Section 2.4). Parameters of the `Mason_simulator` were set at default values.

### 2.4 The Bayes Classifier

Our classifier  $C$  is also employed in Karr et al. (2022a), and is similar to that in Wang et al. (2007). For each read  $R$ , three posterior probabilities are calculated, one for each genome, and the decision for that read is the genome with the maximal posterior probability—the MAP (maximal *a posteriori* probability) estimate. In the notation and terminology of Section 2.1,

- $\mathcal{I}$  is the set of all sequences of length 101 from the set  $\{A, C, G, T, N\}$ ;
- $\mathcal{O} = \{\text{Adeno}, \text{COVID}, \text{SARS}\}$ ;
- $R_1, R_2 \in \mathcal{I}$  are neighbors if and only if  $R_1$  and  $R_2$  differ by exactly one character, i.e., their Hamming distance (Navarro, 2001) is equal to one.

Therefore, each element of  $\mathcal{I}$  has 404 neighbors.<sup>4</sup> Conveniently and importantly, nature provides a physical interpretation of neighbors as SNPs.

There are three likelihood functions, one for each genome, and denoted by  $L(\cdot|\text{Adeno})$ ,  $L(\cdot|\text{COVID})$  and  $L(\cdot|\text{SARS})$ , calculated from the triplet distributions. To illustrate for adenovirus,

$$\begin{aligned}
 L(R|\text{Adeno}) &= P_2(R(1)R(2)|\text{Adeno}) \times T_3((R(1), R(2)), R(3)|\text{Adeno}) \\
 &\quad \times T_3((R(2), R(3)), R(4)|\text{Adeno}) \times \dots \\
 &\quad \times T_3\left((R(|R| - 2), R(|R| - 1)), R(|R|)|\text{Adeno}\right), \tag{3}
 \end{aligned}$$

$P_2(\cdot|A)$  is the pair distribution defined by obvious analogy with (1), and  $T_3$  is given by (2). In (3), we have ignored Ns for simplicity; when they are present, they lead to sums over all possible bases.

To complete the Bayesian formulation, we assume a uniform prior  $\pi_R = (1/3, 1/3, 1/3)$  on  $\mathcal{O}$  for each read. We then use Bayes’ theorem and the three likelihoods to calculate posterior probabilities over  $\mathcal{O}$ ,

<sup>2</sup>Illumina is leading manufacturer of NGSs, producing machines that employ an optical technology; see <https://www.illumina.com/>.

<sup>3</sup>The are cases where the sequencer detects that a nucleotide is present, but is unable to determine whether it is A, C, G or T.

<sup>4</sup>In some settings below, we do not allow Ns, in which case there are 303 neighbors.

which yield the classifier decisions. Specifically, for each read  $R$ , the posterior probability of  $x \in \mathcal{O}$  is given by

$$p(x|R) = \frac{\pi_R(x)L(R|x)}{\pi_R(\text{Adeno})L(R|\text{Adeno}) + \pi_R(\text{COVID})L(R|\text{COVID}) + \pi_R(\text{SARS})L(R|\text{SARS})}. \quad (4)$$

Finally,

$$C(R) = \arg \max_{x \in \mathcal{O}} p(x|R).$$

We note that since the  $\pi_R$  is uniform, it cancels in (4), so  $C(R)$  is also the maximum likelihood estimator (MLE). Terming  $C$  a naïve Bayes classifier reflects that there is no borrowing of strength across reads.

## 2.5 The Boundary

We now define the boundary  $\mathcal{B}$  associated with  $C$  to be the set of elements of  $\mathcal{I}$  that have at least one neighbor classified differently:

$$\mathcal{B} = \{R \in \mathcal{I} : C(R') \neq C(R) \text{ for some } R' \in N(R)\}. \quad (5)$$

In principle, the notation should capture dependence of the boundary on  $C$ , but in this case study,  $C$  is fixed, so we suppress that dependence.

Perhaps the most salient observation in this paper is that *whenever two reads are classified differently, any graph path in  $\mathcal{I}$  connecting them must contain at least two boundary points*. Below we focus on *Hamming paths*, which are the shortest. Given reads  $R \neq R'$  with Hamming distance  $k$ —they differ in  $k$  of 101 locations, a Hamming path from  $R$  to  $R'$  simply replaces one nucleotide in  $R$  at a time by the corresponding nucleotide in  $R'$ . Therefore, each successive pair on the path are neighbors. Such a path  $(R_0 = R, \dots, R_k = R')$  has length  $k + 1$ ; there are  $k!$  of them. The “simplest” path simply moves left to right in the character strings. Because  $C(R) \neq C(R')$ , there must be at least one value of  $j$  for which  $C(R_j) \neq C(R_{j+1})$ , in which case,  $R_j$  and  $R_{j+1}$  are neighbors and both belong to  $\mathcal{B}$ .

To provide some numerical evidence, Table 1 contains the confusion matrix for the Bayes classifier  $C$ , which is computable because we know the source of each read, and shows that  $C$  performs well, albeit not spectacularly. Looking only at the columns, Table 1 identifies

- 3, 867, 933 = 1933  $\times$  2001 pairs, the first of which is classified as Adeno and the other as COVID;
- 3, 740, 355 = 1933  $\times$  1935 pairs, the first of which is classified as Adeno and the other as SARS;
- 3, 871, 935 = 2001  $\times$  1935 pairs, the first of which is classified as COVID and the other as SARS.

Any enthusiasm about the size of these numbers should be tempered by remembering that  $|\mathcal{I}| = 5^{101}$ .

## 2.6 Surrogate Uncertainty Measures

As we investigate in more detail in Section 3.1, the Bayes classifier  $C$  possesses two related inherent measures of uncertainty, the maximum of the three posterior probabilities and the entropy of the posterior distribution. Other classifiers lack such measures, although sometimes there are informal measures of “confidence.” We now introduce two surrogate measures that are computable for *any* classifier operating on the same input space  $\mathcal{I}$ .

Table 1: Confusion matrix for the Bayes classifier  $C$ . The correct classification rate is 81.55%.

Source	Decision			Sum
	Adeno	COVID	SARS	
Adeno	1601	115	250	1966
COVID	64	1717	215	1996
SARS	268	169	1470	1907
Sum	1933	2001	1935	5869

The first, which we term *Neighbor Similarity*, quantifies the extent to which the neighbors of a read have the same decision it does. In symbols, given a read  $R$ ,

$$\text{NS}(R) = 1 - H(q_R, q_{N(R)}), \quad (6)$$

where  $H$  denotes Hellinger distance (Nikulin, 2001),  $q_R$  is the generate probability distribution on  $\mathcal{O}$  concentrated on  $C(R)$ , and  $Q_{N(R)}$  is the probability distribution on  $\mathcal{O}$  of  $\{C(R') : R' \in N(R)\}$ . The Hellinger distance between distributions  $p$  and  $q$  on a finite set  $A$  is given by

$$H(p, q) = \sqrt{\frac{1}{2} \sum_{x \in A} \left( \sqrt{p(x)} - \sqrt{q(x)} \right)^2}. \quad (7)$$

Hellinger distance is a metric, and takes values between zero—if and only if  $p = q$ —and one, the latter when  $p$  and  $q$  have disjoint supports. The greater  $H(p, q)$ , the more different are  $p$  and  $q$ . Then in symbols,

$$\mathcal{B} = \{R \in \mathcal{I} : \text{NS}(R) < 1\}. \quad (8)$$

Note that NS only takes account of how many neighbors differ, and not what their values are.

The interpretation of  $\text{NS}(R)$  is uncertainty regarding the classification of  $R$ . If  $\text{NS}(R) = 1$ , *all* neighbors of  $R$  have the same decision as  $R$ , and we can be more certain of the decision for  $R$ . At the other extreme, if  $\text{NS}(R)$  is zero,<sup>5</sup> *no* neighbor of  $R$  has the same decision: changing any single nucleotide of  $R$  changes the decision, in which case we should be highly uncertain about  $C(R)$ . In Section 3.1, we investigate the relationship between NS and the inherent measures of uncertainty for  $C$ .

Note that  $\text{NS}(\cdot)$  can be calculated for any classifier whose input space has the graph structure described in Section 2.1, and its value returned along with the classifier decision. The “only” burden is computational: the classifier must be run on all neighbors of the input, of which there may be many. Even in our relatively simple case study, without parallelization, the run time is increased by a factor of 400. See Section 4 for further discussion.

The second surrogate measure is equally intuitive but more speculative, because we lack a demonstrably feasible method for calculating it. It the *distance from the boundary*:  $\text{DB}(R)$  is the minimum value of  $k$  for which there exists a path  $(R_0 = R, \dots, R_k)$  in  $\mathcal{I}$  such that  $R_k \in \mathcal{B}$ . Then, the interpretation is that the larger  $\text{DB}(R)$ , the greater the certainty regarding  $C(R)$ , because the more  $R$  would have to be “mutated” in order

<sup>5</sup>Which does not occur in our case study.

to change  $C(R)$ . It is easy to obtain upper bounds on  $C(R)$ : for any other read  $R'$  with  $C(R') \neq C(R)$ ,  $DB(R)$  is at most the Hamming distance between  $R$  and  $R'$ . The unresolved problem is exact computation of  $DB(R)$ .

### 3 Results

All analyses reported here were performed using the R Language and Environment for Statistical Computing (R Core Team, 2020). Data and R code are available at TBD.

#### 3.1 DNA Reads

Table 2 contains cross-tabulations of the boundary status for the 5869 reads as a function of read source, the classifier decision and correctness of the classifier decision. Before discussing details, we observe, possibly startlingly, that 1791 of the 5869 reads, or 30.52%, lie on the boundary  $\mathcal{B}$ , the first concrete evidence of our assertion that  $\mathcal{B}$  is not “thin.” Of these 1791 boundary reads, 190 have neighbors classified as both other genomes, making them in some sense triple points.

Looking in more detail, Figure 1 shows the neighbor distributions over  $\mathcal{O}$  for all the reads. In it, three-dimensional probabilities (barycentric coordinates) are converted to Cartesian coordinates, as points in an equilateral triangle. Pure Adeno, in the sense that  $\text{Prob}(\text{Adeno}) = 1$ , is the top vertex, pure COVID is the lower left vertex, and pure SARS is the lower right vertex. Because we know the sources of the reads, we create separate displays for each source. The white diamond in each scatterplot is the centroid of the probabilities it contains, and all three centroids lie close to the source. A read on an edge has neighbors of two kinds, one of which is that of the read itself. (The bizarre case of a read classified differently from all of its neighbors does not occur in our dataset. The minimum number of concordant neighbors is 11.) A read in the interior of the triangle has neighbors with all three decisions.

The topmost table in Table 2 shows boundary status as a function of read source, so that its row sums match those in Table 1. In it, Boundary Status is the number genomes other than that of the read appearing among the neighbors. Thus, 0 means all neighbors are classified the same as the read, i.e., it is not on the boundary; 1 means one of the other genomes appears among the neighbors, and 2 means that both other genomes appear among the neighbors. The distribution of Boundary Status is not uniform across the three sources: boundary percentages are 30.0% for Adeno reads, 22.1% for COVID reads and 40.0% for SARS reads. The  $p$ -value for the  $\chi^2$  test on this table is less than  $10^{-16}$ . SARS reads are more likely than others to lie on the boundary, which is consistent with findings in (Karr et al., 2022a) regarding difficulties in classifying them.

The middle table in Table 2 provides a complementary view of boundary status as a function of classifier decision, so that its row sums match the *column sums* in in Table 1. Here also, the  $\chi^2$  test is massively significant. SARS remains the outlier: relatively more reads classified as SARS lie on the boundary than for Adeno or COVID.

The bottom table in Table 2 shows boundary status as a function of correctness of the classifier decision, and begins to get at the heart of the matter. Of incorrectly decided reads, 64.66% lie on the boundary, while only 22.81% of correctly decided reads lie on the boundary! The classifier is struggling in the vicinity of  $\mathcal{B}$ , and one rightly should be less confident of such decisions. The  $\chi^2$  statistic for this table is 726.65, more than five times that for source (topmost table), and three times that for decision (middle table). Moreover,

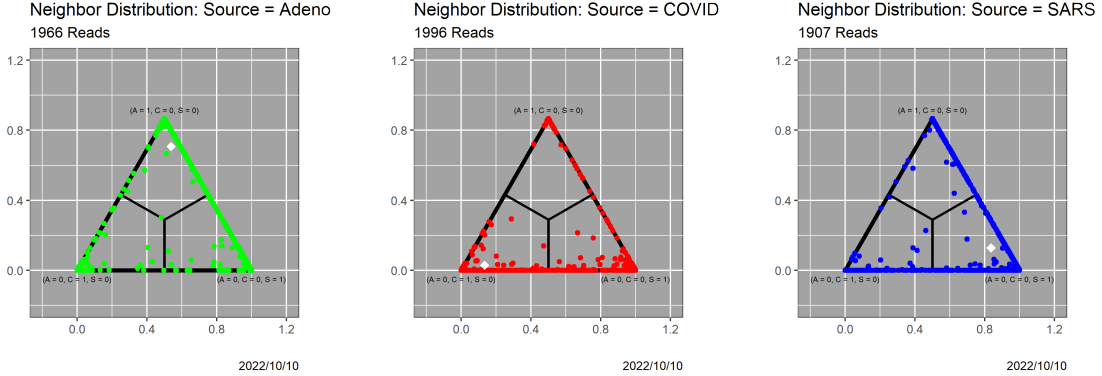


Figure 1: Neighbor distributions for the 5869 reads, by source.

the Kolmogorov-Smirnov test for the two empirical cumulative distribution functions (ECDFs) is massively significant: NS is lower for incorrect decisions than for correct ones.

To make things more precise, we next examine Neighbor Similarity. In parallel to Table 2, Figures 2–4 show the distribution of Neighbor Similarity, as defined by (6), as a function of read source, read decision and decision correctness, respectively. Each contains plots of both density functions and ECDFs. In particular, the ECDFs make clear the numbers of reads that are not on the boundary, for which  $NS(R) = 1$ . The qualitative messages mirror those in Table 2.

Neighbor Similarity is, at least relatively, much more burdensome computationally than simply running the classifier. In our case study, a classifier that requires an hour to run would, if it also were to provide Neighbor Similarity, require 17 days. For the image analysis example in Section 2.1, the multiplier (ignoring edge effects) is 1,572,864, which is ridiculous.<sup>6</sup> Confronting the problem directly requires only observing that the computation is infinitely parallelizable: classifier evaluation for one neighbor is completely independent of that for other neighbors.

An alternative strategy is to sample neighbors, which generates estimates for Neighbor Similarity. Figure 5 provides initial evidence that sampling can be effective. It is based on the entire 5869-element read dataset. The  $x$ -axis is the number of reads sampled; the order was randomized for each read. The  $y$ -axis is more complicated. For each read  $R$  and sample size  $k$  we calculated a partial Neighbor Similarity  $NS(R, k)$  using (6). Then for each  $k$ , we fitted a linear model with  $NS(\cdot, 404) = NS$  as response and  $NS(\cdot, 1), \dots, NS(\cdot, k)$  as predictors. Finally, the  $y$  axis contains values of relative root mean squared error (RRMSE)<sup>7</sup> for each model. From the figure, an RRMSE of 5% requires only 20 sampled neighbors, and there is minimal benefit from sample sizes exceeding 80. How these values scale with problem size is not clear. The hypothesis that they scale linearly is less than what one would wish.

We next investigate the relationships between the surrogate measures of uncertainty introduced in Section 2.6 and two inherent measures for  $C$ : the maximum of the three posterior probabilities and the entropy of the posterior distribution. The former is defined by

$$MP(R) = \max \{p(\text{Adeno}|R), p(\text{COVID}|R), p(\text{SARS}|R)\}, \quad (9)$$

<sup>6</sup>For the record, an hour becomes 180 years.

<sup>7</sup>The square root of the mean squared error for the linear model divided by the mean response.

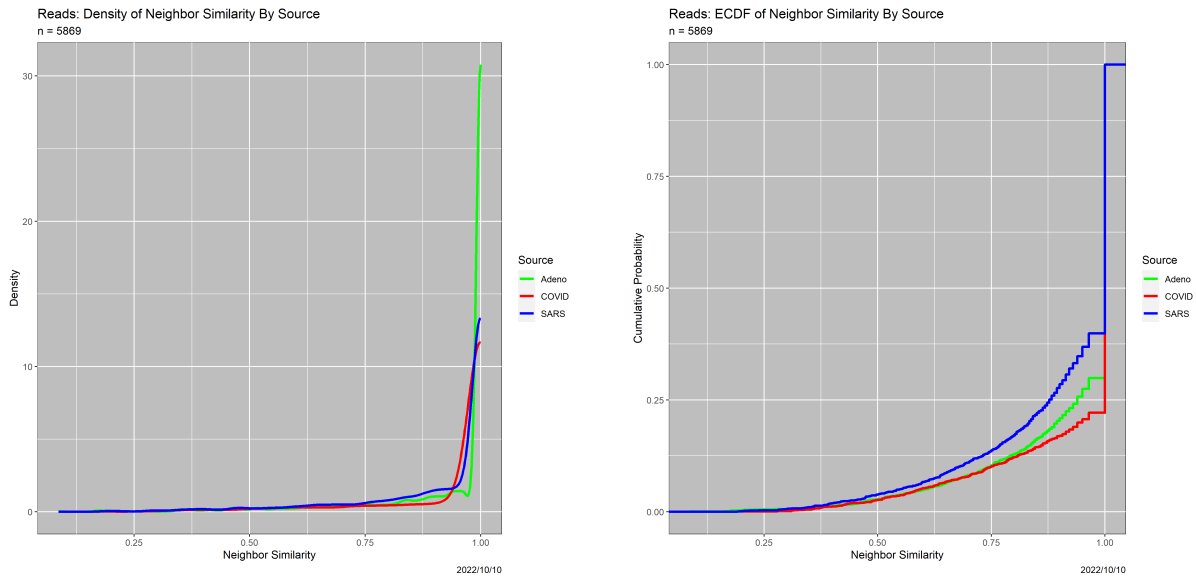


Figure 2: *Left*: Densities of Neighbor Similarity by read source. *Right*: ECDFs of Neighbor Similarity by read source.

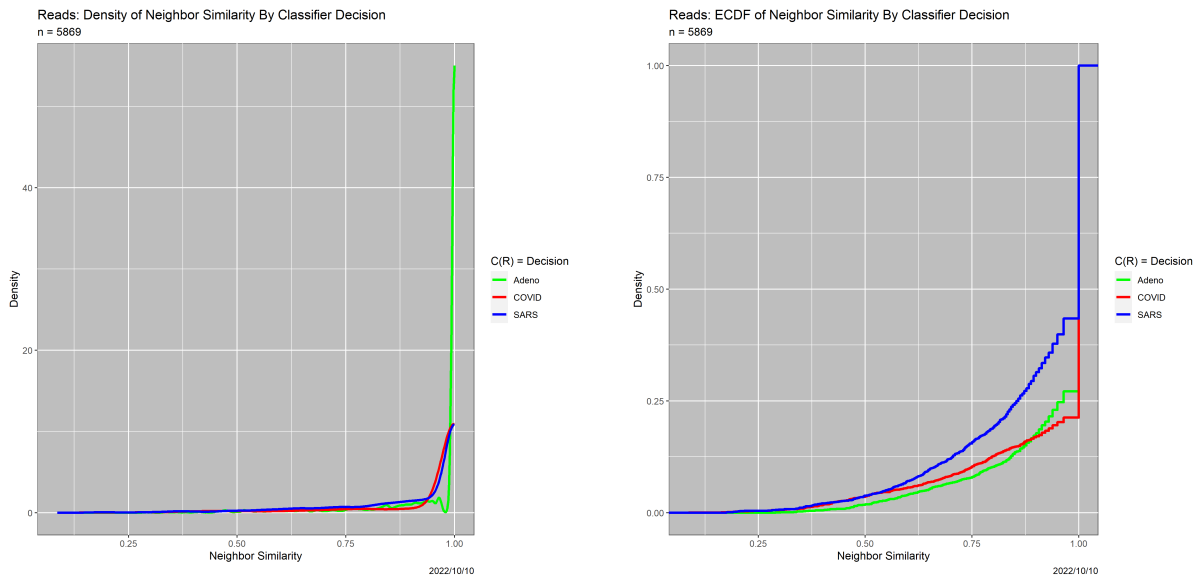


Figure 3: *Left*: Densities of Neighbor Similarity by classifier decision. *Right*: ECDFs of Neighbor Similarity by classifier decision.

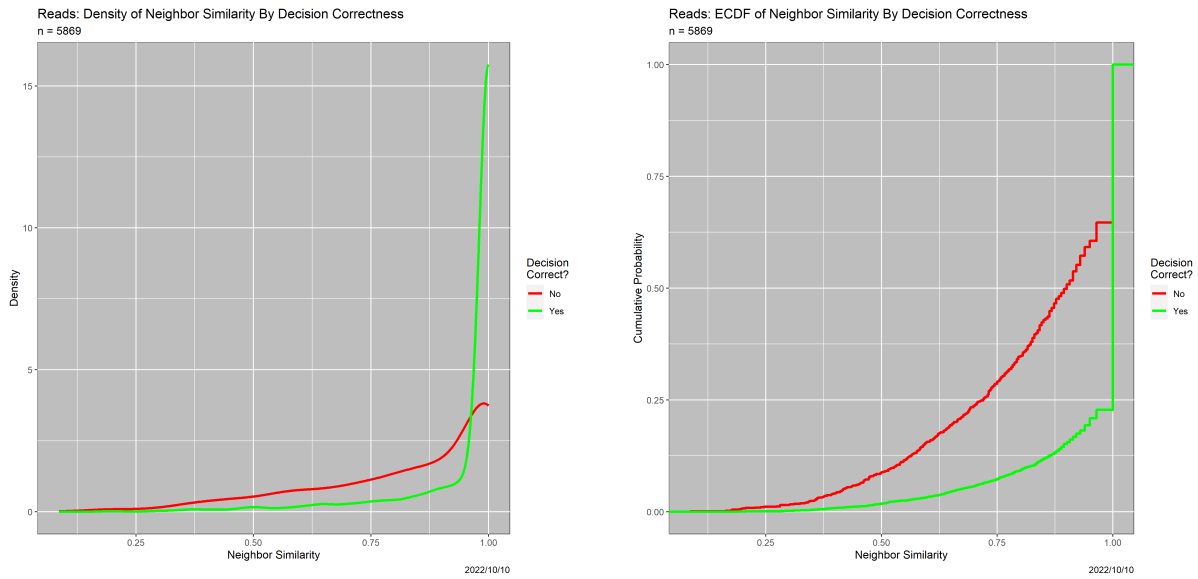


Figure 4: *Left:* Densities of Neighbor Similarity by decision correctness. *Right:* ECDFs of Neighbor Similarity by decision correctness.

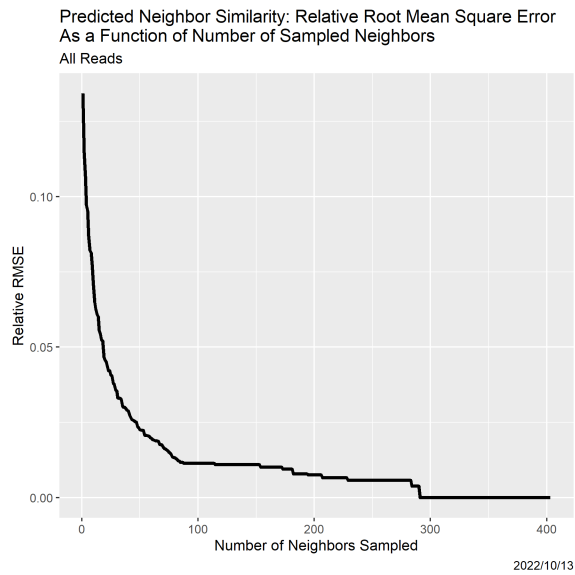


Figure 5: Relative root mean squared error in estimating NS from samples of neighbors.

Table 2: *Top*: Cross-tabulation of read source and boundary status. *Middle*: Cross-tabulation of read decision and boundary status. *Bottom*: Cross-tabulation of decision correctness and boundary status.

Source	Boundary Status			Sum
	0	1	2	
Adeno	1378	526	62	1966
COVID	1554	375	67	1996
SARS	1146	700	61	1907
Sum	4078	1601	190	5869

Decision	Boundary Status			Sum
	0	1	2	
Adeno	1408	491	34	1933
COVID	1575	345	81	2001
SARS	1095	765	75	1935
Sum	4078	1601	190	5869

Correct? Decision	Boundary Status			Sum
	0	1	2	
No	382	598	101	1081
Yes	3696	1003	89	4788
Sum	4078	1601	190	5869

where the posterior distribution  $p(\cdot|R)$  is given by (4). Always,  $MP(R) \geq 1/3$  and the closer  $MP(R)$  to 1, the more certain  $C$  is of the decision for  $R$ . Thus, MP and NS should be directly related. Figure 6 shows that, indeed, they are, and strongly so. It depicts the relationship between MP and NS as a function of classifier decision. Because our ultimate goal is to employ NS in contexts where neither MP nor a model-derived analog is available, it would not have been appropriate to use read source there rather classifier decision. The correlation between MP and NS is 0.8488; the disaggregated correlations are 0.8784 for Adeno, 0.8502 for COVID and 0.8400 for SARS.

We can construct good statistical models to predict  $MP(R)$  from  $NS(R)$  and  $C(R)$ , of which we present two. The first is a fully saturated quadratic model reflecting the curvature evident in Figure 6:

$$MP = \alpha_{C(R)}NS(R)^2 + \beta_{C(R)}NS(R) + \gamma_{C(R)}. \quad (10)$$

As the notation suggests, the process is equivalent to fitting three separate models to datasets constructed by filtering on  $C(R)$ . The adjusted coefficient of determination  $R^2$  for the model is 0.8341, indicating good fit. Figure 7 shows actual and predicted values of MP by classifier decision. Table 3 contains the estimated values of the coefficients.

As noted previously, NS effectively counts the number of differently classified neighbors, and is therefore discrete, although numerically-valued. Consequently, much of the imperfect fit is simple inability to predict the continuous variable MP within sets of reads having the same value of NS (especially those the

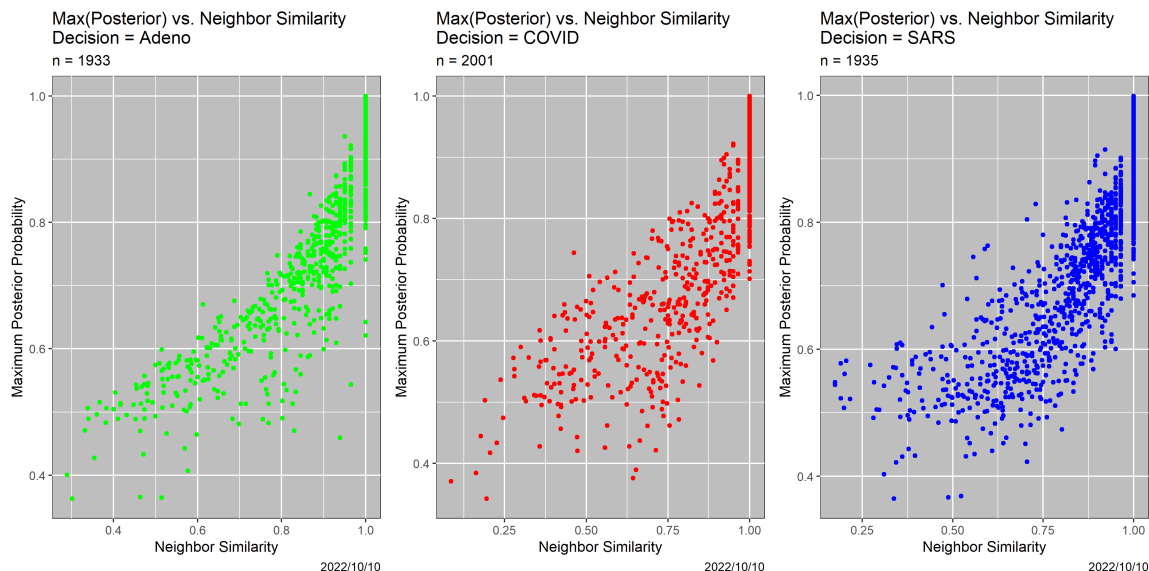


Figure 6: Scatterplots of MP versus NS, by classifier decision. *Left*: decision = Adeno, *Center*: decision = COVID. *Right*: decision = SARS.

NS = 1), as the figure makes perfectly clear. Thus, a second predictor would be valuable: DB is a promising candidate, but not yet viable computationally. It also is integer-valued, and so does not obviate the discreteness problem with NS.

Figure 8 shows a partition model, in this case a regression tree (Breiman et al., 2017; Hastie et al., 2001), whose mean squared error matches that of the quadratic model. The tree has been pruned to only seven terminal nodes using standard heuristics that trade off predictive accuracy for model complexity. The mean squared error for the partition model is actually slightly superior to that for the regression model—0.003313057 as compared to 0.003794415.

The second inherent measure of uncertainty for  $C$  is *posterior entropy* PE.<sup>8</sup> Analogously to Figure 6, Figure 9 contains scatterplots of PE versus NS by classifier decision. Possibly disappointingly but at least informatively, PE is predicted significantly less well by NS and classifier decision than is MP. For a quadratic regression model analogous to that in (10), the adjusted  $R^2$  is only 0.6928. The corresponding partition model, shown in Figure 10, shows which variables and interactions are most relevant. Again, the mean squared error for the partition model is slightly lower than for the quadratic regression model.

### 3.2 Exploring the Boundary

We present here three strategies, one with two variants, for identifying elements of the boundary  $\mathcal{B}$  and exploring the structure of  $\mathcal{B}$ .

<sup>8</sup>The entropy of a probability distribution  $P$  on a finite set  $\mathcal{S}$  is  $H(P) = -\sum_{s \in \mathcal{S}} p(s) \log p(s)$ , with the convention that  $0 \times -\infty = 0$ . Entropy is minimized by distributions concentrated at a single point and maximized at the uniform distribution on  $\mathcal{S}$ , with maximizing value  $\log(|\mathcal{S}|)$ .

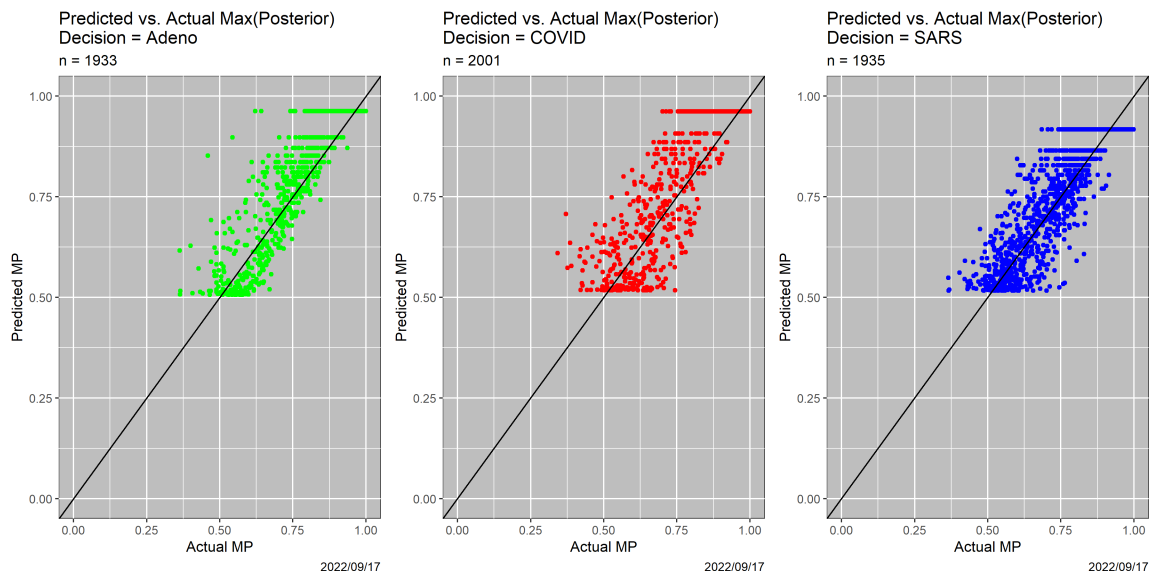


Figure 7: For the quadratic regression model, scatterplots of predicted MP versus actual MP, by classifier decision. *Left*: decision = Adeno, *Center*: decision = COVID. *Right*: decision = SARS.

Finding boundary points is easy: the first and simplest method has been mentioned already in Section 2.5: if  $C(R) \neq C(R')$ , then any path from  $R$  to  $R'$  contains at least two elements of  $\mathcal{B}$ . For the reads dataset, there are 11,480,223 such pairs. If we eliminate duplicates and for each pair consider only the Hamming path that in (“left-to-right”) order replaces each nucleotide in  $R$  differing from the corresponding nucleotide in  $R'$  by the latter, then we have a surprisingly effective mechanism for locating boundary pairs. Based on an small random sample of 25 origin reads, but considering *all other reads with different decisions*, 1,242,162 boundary points were identified. There is significant variability, however, as shown in Table 4. Moreover, as is clear from Figure 11, paths originating from reads classified as COVID differ significantly from those originating at reads classified as Adeno or SARS.

Of course, whenever  $C(R) \neq C(R')$ , there are multiple (minimal length) Hamming paths connecting  $R$  and  $R'$ . Indeed, if  $k$  is the Hamming distance between  $R$  and  $R'$ , then there are  $k!$  such paths, corresponding to all possible orderings of replacement for the sites where  $R$  and  $R'$  differ. Limited experiments have shown that a strategy of using multiple Hamming paths is not materially more effective than using one Hamming path in terms of unique boundary pairs identified relative to computational effort. The reason, we believe, is that multiple paths from  $R$  to  $R'$  often cross  $\mathcal{B}$  at the same places.

A second strategy motivated by Markov chain Monte Carlo (MCMC) methods used under the rubric algebraic statistics to investigate large spaces of contingency tables (Diaconis and Sturmfels, 1998) is to perform random walks originating from sequences  $x \in \mathcal{I}$ , moving to a neighboring sequence at each step, and checking whether  $\mathcal{B}$  has been crossed, i.e., whether the classifier decision has been changed. Were  $\mathcal{B}$  thin, this strategy of wandering randomly would be horribly inefficient. But, because  $\mathcal{B}$  is not thin, it works reasonably well. To illustrate, we chose a random sample of 100 reads for each decision, and ran random walks of length 2000 steps originating at each. Keeping in mind that each boundary pair comprises two

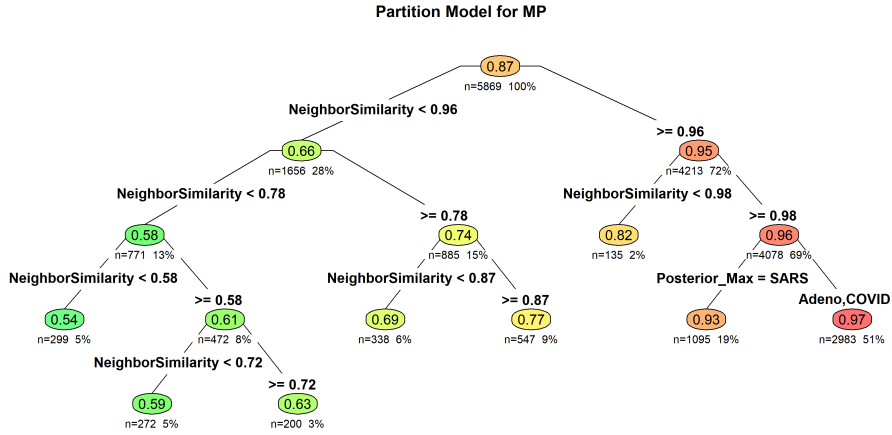


Figure 8: Partition model for  $MP(R)$  using  $NS(R)$  and  $C(R)$  as predictors. Values in each node are means of  $MP$ ; numbers below nodes are counts and percentages; edges are labeled by the predictor on which the split occurs and the associated value.

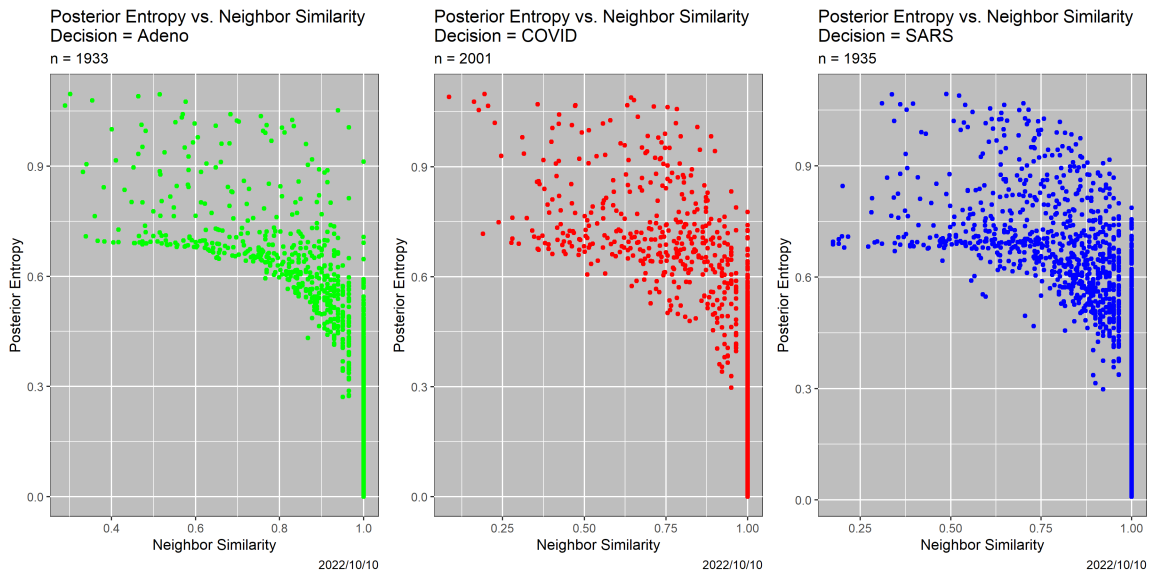


Figure 9: Scatterplots of PE versus NS, by classifier decision. *Left:* decision = Adeno, *Center:* decision = COVID. *Right:* decision = SARS.

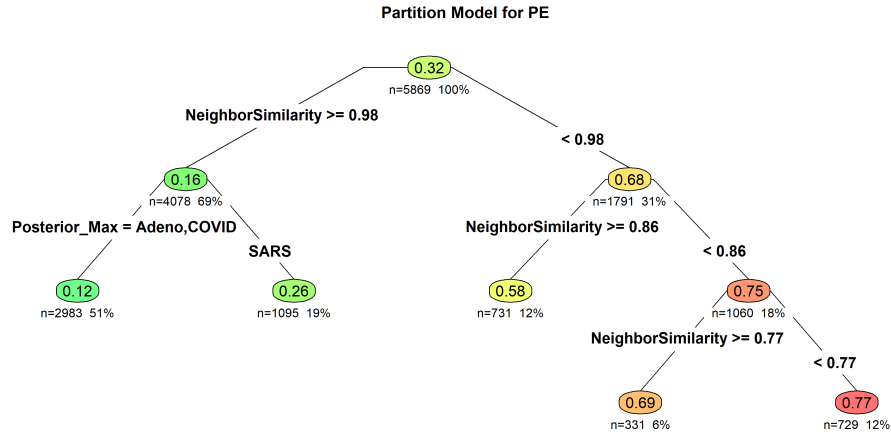


Figure 10: Partition model for  $PE(R)$  using  $NS(R)$  and  $C(R)$  as predictors. Values in each node are means of  $PE$ ; numbers below nodes are counts and percentages; edges are labeled by the predictor on which the split occurs and the associated value.

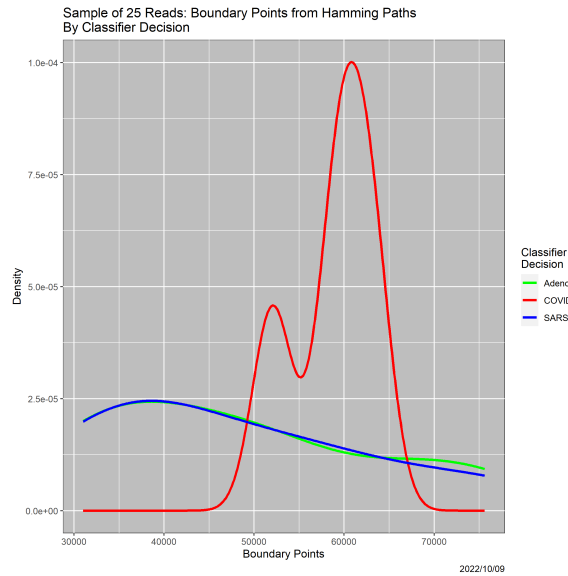


Figure 11: Numbers of boundary points on Hamming paths, by classifier decision.

Table 3: Estimated coefficients for the quadratic regression model with  $MP(R)$  as response and  $NS(R)$  and  $C(R)$  as predictors. All coefficients except are statistically significant at level 0.001.

Coefficient	Value
$\alpha_{\text{Adeno}}$	2.07873
$\alpha_{\text{COVID}}$	1.45459
$\alpha_{\text{SARS}}$	1.49852
$\beta_{\text{Adeno}}$	-2.20866
$\beta_{\text{COVID}}$	-1.44745
$\beta_{\text{SARS}}$	-1.5496
$\gamma_{\text{Adeno}}$	1.09297
$\gamma_{\text{COVID}}$	0.80804
$\gamma_{\text{SARS}}$	0.86606

boundary points, 35,352 boundary points were found, of 600,300 sequences visited. For comparison, we repeated the experiment starting from 300 sequences known to be boundary points, again spread uniformly over the three decisions. The improvement over random walks starting from random sequences is minimal; indeed, fewer boundary points—35,238—were identified. It is noteworthy, however, that *none* of the 600 random walks failed to cross the boundary, so it is never far away. Summary statistics appear in Table 5.

From Table 6, both versions of random walks are less efficient than Hamming paths, as measured by the number of boundary points identified divided by the number of classifier evaluations. This measure rests on the completely plausible assumption that classifier evaluation is the primary computational expense of boundary exploration, as discussed in Section 2.3. But, these results confirm the ubiquity of  $\mathcal{B}$ .

Note that both Hamming paths and random walks may pass through boundary points without identifying them, which can happen because each point in the path is compared only to its predecessor rather than all of its neighbors.

Finally, we present random walk-like methods for "crawling the boundary" once it has been reached. The motivation should be clear: from a point on the boundary, it should be possible to crawl along the boundary, which indeed it is. More precisely, we simulated 100 random walks starting at boundary points, but constrained to move only to adjacent and not previously visited boundary points. Each crawl was allowed to continue for 250 steps, or until it was not possible to move to another—we remind, not previously visited—boundary point. The fact that such points exist further confirms the geometric complexity of the boundary: it is "hairy."

Crawling the boundary clearly is insightful, but it is not efficient. Of the 100 random walks, 64 did not terminate within 250 steps, indicating that the boundary  $\mathcal{B}$  is, as one would expect a boundary to be, significantly contiguous. The lengths of crawls that did terminate range from 5 to 242, with no discernible structure to their distribution. These 36 crawls are the hairs mentioned in the preceding paragraph—points at which continuing on the boundary is possible only by backtracking. While in the minority, they are nevertheless not rare, so the boundary *is* hairy. Beyond this, the boundary is convoluted: all three decisions are present in 58 of 100 crawls. Put different, if one were to think of three boundaries—an Adeno–COVID boundary, an Adeno–SARS boundary, and a COVID–SARS boundary—they cross each other frequently, as evidenced by the 190 reads with neighbors of all three types. In all other crawls, the decisions must and do

Table 4: Results for Hamming paths from 25 randomly sampled reads to all other reads with differing classifier decisions.

SampleID	Decision	Boundary Points	Classifier Evaluations
958	Adeno	71646	296286
1283	SARS	59530	298994
256	Adeno	50388	294923
1137	SARS	32052	303790
638	SARS	75160	296341
4905	Adeno	57804	302409
2914	Adeno	42374	292198
513	COVID	63228	289336
2160	COVID	52038	292711
2835	COVID	58806	293286
1386	Adeno	31784	304305
3584	Adeno	40992	296839
1912	SARS	34274	296172
4857	Adeno	31002	302553
3713	Adeno	37630	292638
4196	Adeno	32332	300289
5113	Adeno	68118	293587
4090	SARS	43252	297002
1981	Adeno	49500	293600
2666	Adeno	50380	295404
2153	COVID	60832	295370
2674	SARS	52446	295611
351	Adeno	75608	301328
5154	SARS	37546	297293
1940	Adeno	33440	303009

alternate, indicating that some segments of the boundary are between two decisions.

The inefficiency of crawling the boundary, which is apparent in Table 6, is partly an artifact of our computational implementation. At each step, we classify *all* neighbors before determining if it is possible to proceed. Computation would clearly be reduced by examining neighbors sequentially, and proceeding once a neighbor with a differing classification is identified, but the reduction in effort has not been explored. More detailed boundary crawl results appear in Tables 11 and 12 in Appendix B.

### 3.3 Do Boundary Points Differ from Other Sequences?

Our final results address a natural question of whether boundary points differ from other sequences. We focused on real (modulo `Mason_simulator` synthesis) as opposed to random DNA sequences: do the 1791 boundary reads differ from the 4078 other reads?

Table 5: Comparison of summary statistics for 300 random walks originating at reads and for 300 random walks originating at boundary points.

Origins	Minimum	Mean	Maximum
Reads	28	117.77	274
Boundary Points	16	117.46	280

Table 6: Summary of methods for exploring the boundary.

Method	Classifier Evaluations	Boundary Points	Efficiency
Hamming Paths	7,425,274	1,242,162	16.73%
Random Walks, Random Origin	600,300	34,932	5.82%
Random Walks, Boundary Origin	600,300	25,238	5.87%
Crawling Boundary	8,146,256	20,164	0.25%

To address it, we first apply the hierarchical clustering strategy using triplet distributions employed in for outlier identification in Karr et al. (2022a). The clustering is performed with the `hcluster` package in R, using “complete” clustering. By means of standard heuristics, the resultant dendrogram was pruned to the 21 clusters shown in Table 7. Overall, 30.52% of the reads are on the boundary; in many clusters the percentage of reads belonging to  $\mathcal{B}$  is quite different. In particular, six clusters, albeit small, contain *no* boundary points, while more than 60% of the reads in another cluster belong to  $\mathcal{B}$ .

Nevertheless, the results in Table 7 are not overwhelming: there is signal, but not strong. A partition model tells a complementary story. That model, fitted to the reads and employing standard pruning heuristics, contains 627 terminal nodes and fits the read data essentially perfectly, as shown in Table 8. One should not be overwhelmed, however, by the correct classification rate of 99.27%, because always predicting “not on the boundary” is correct for 69.38% of reads. Only 236 terminal nodes are required in order to attain a rate of 90%. The partition model does not, moreover, predict accurate for data other than those to which it was fit. Applied to a dataset of 7493 sequences generated by random walks of length 25 starting at 300 reads, and so not straying too far from the reads, the correct classification rate is only 63.33%. It seems clear that no generalizable model can be based on such a small sample of  $\mathcal{I}$ .

## 4 Discussion

### 4.1 General Issues

There are two themes in this paper: the nature of the boundary and the proposed surrogate measures of uncertainty, especially Neighbor Similarity.

Concerning the former, the takeaway message is “beware the boundary.” For our Bayes classifier, all analyses we have conducted suggest that the boundary may comprise 20% or more, of the input space. And not only is the boundary not sparse, but also it is geometrically complicated, even hairy. There is temptation

Table 7: Distribution of boundary points in each of the 21 triplet distribution clusters.

Cluster	Boundary	Not Boundary	Percent Boundary
1	45	211	17.58
2	298	411	42.03
3	419	816	33.93
4	261	322	44.77
5	12	28	30.00
6	187	383	32.81
7	5	30	14.29
8	79	104	43.17
9	248	416	37.35
10	12	161	6.94
11	53	110	32.52
12	0	48	0.00
13	42	96	30.43
14	0	18	0.00
15	1	14	6.67
16	103	857	10.73
17	0	3	0.00
18	0	26	0.00
19	0	4	0.00
20	26	17	60.47
21	0	3	0.00

to call it fractal-like, but doing so is a misnomer in the sense that the multiscale character of fractals has no analog for classifier boundaries.

The extent to which lying on or near  $\mathcal{B}$  can or should affect either classifier output or decisions based on it is clearly contextual. The first issue is whether to check boundary status for a given query. So long as the input space has the graph structure, the only issue is computational: simply check all the neighbors, which is completely parallelizable, but may be daunting. If one cares only about whether the query is on the boundary, the process can be terminated once a neighbor with a different result is found. We posit that in many cases, both scientific and broader impacts merit a numerical measure such as Neighbor Similarity. Perhaps in our read classification example, which is conceptually part of metagenomic assembly, the consequences of misclassification are not major. For classifications such as SeqScreen (Balaji et al., 2022), which is meant to identify pathogenic sequences, the consequences of incorrect decisions may be dramatic, and the risks of accepting high-uncertainty classifier results without further investigation may be unacceptable.

Furthermore, in the face of rampant concern about data quality in DNA databases (Commichaux et al., 2021; Langdon, 2014; Steinegger and Salzberg, 2020), and given that changing data point to a neighbor, as done in (Karr et al., 2022b) to measure data quality, is the smallest conceivable data quality problem,<sup>9</sup> it

<sup>9</sup>As least with respect to the accuracy dimension of data quality, which is but one of many dimensions (Karr et al., 2006).

Table 8: Confusion matrix for partition model, for 5869 reads, of boundary status as a function of triplet distribution. The correct classification rate is 99.27%.

Actual	Modeled		Sum
	No	Yes	
No	4056	22	4078
Yes	21	1770	1791
Sum	4077	1792	5869

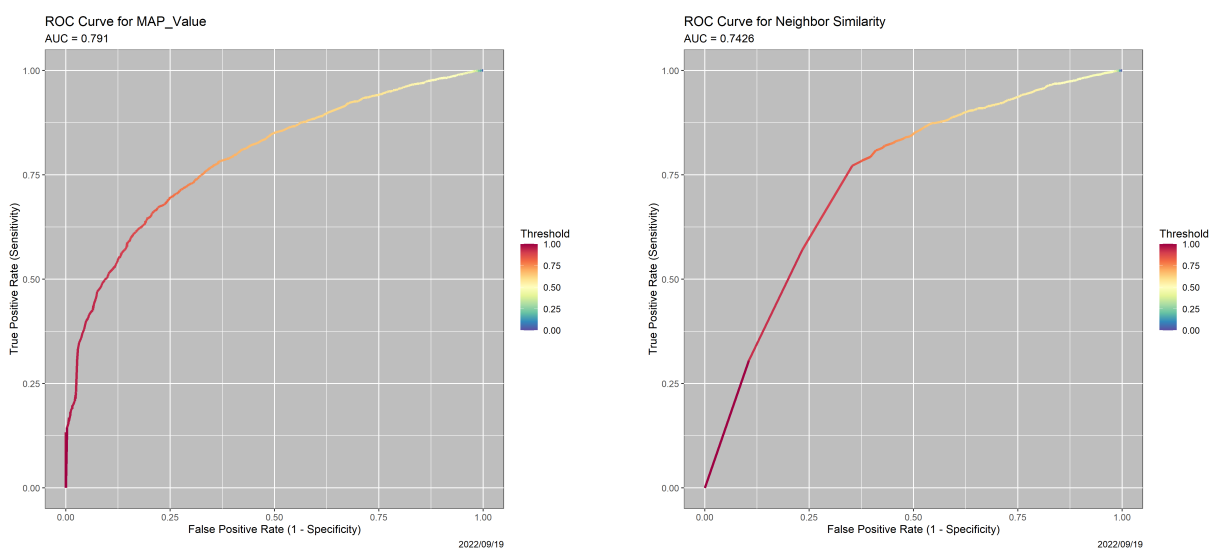


Figure 12: *Left*: ROC curve for the decision rule based on thresholded values of MAP. *Right*: ROC curve for the decision rule based on thresholded value of NS.

seems only prudent to care about neighbors.

In Section 3, we showed that that Neighbor Similarity relates in a describable way to both inherent measures of uncertainty for our Bayes classifier. From an operational perspective, Figure 12 is more important. It contains receiver operating characteristic (ROC) curves for two decision rules, one based on accepting decisions for which MAP exceeds a threshold, which is encoded by color, the other for the decision rule based on accepting decisions for which NS exceeds a threshold. The two ROC curves are essentially identical. For the Bayes classifier, NS is as effective as MAP.

## 4.2 Other Datasets

There is, of course, an obvious question of scientific generalizability. It is unclear, *a priori*, whether properties observed for reads, for instance, the distribution of NS, are somehow specific to our read dataset, or descriptive of the classifier  $C$  more generally. To address this question, we ran the classifier on five

additional datasets:

**ReadsNew:** A dataset containing 2000 Adeno reads, 2000 COVID reads and 2000 SARS reads, all of length 101, generated by the `Mason_simulator`, which can be reviewed as addressing the question of replicate variability. There is no reason to expect the classifier to perform differently on it from its performance on the main dataset.

**ReadsEcoli:** A dataset containing 6000 `Mason_simulator`-generated reads of length 100 from an *E. coli* genome. We had no clear expectation of how the classifier would perform on it.

**Random6K:** A dataset containing 6000 random sequences of length 101 generated from {A, C, G, T}, which represents pure noise.

**ReadsMixed1:** A dataset combining the original dataset and 2000 elements of **ReadsEcoli**, which represents a situation the classifier is not prepared for: the presence of a fourth source of reads.

**ReadsMixed2:** A dataset combining the original dataset and 100 elements of **ReadsEcoli**, which represents an alternative situation the classifier is not prepared for: contamination from a fourth source of reads.<sup>10</sup>

The results, including the core dataset **ReadsOriginal** for easy comparison, appear in Table 8 and Figure 13. In Table 8, the three columns under “Decisions” are percentages of the classifier output, as are the two columns under “Boundary.” As intimated, the first two rows, representing two sets of reads from Adeno, COVID and SARS with approximately equal distributions of the read source, do not differ, meaning the that classifier seems not to be vulnerable to replicate variability. The last two rows are the most different from **ReadsOriginal**, and both the Decision distribution and the Boundary distribution differ dramatically from the first two rows. For reasons that are not yet clear, **ReadsEcoli** and **Random6K** are overwhelmingly classified as Adeno. The hypothesis that this constitutes a “vote splitting” artifact of there being one Adenovirus genome and two Coronavirus genomes is demonstrably false. In a set of 30,000 random sequences, if classifier choices are restricted to Adeno and Corona, only 77 of the 27,492 sequences classified as Adeno change to the latter. But **ReadsEcoli** and **Random6K** also differ: using Hellinger distances and empirical  $p$ -values, the differences between the Decision distributions and Boundary distributions are massively significant.

The third and fourth rows in Table 8 are, as expected, midway between the first two rows and the last two rows. Note that, for ease of interpretation, row 3 contains **ReadsMixed2**—the case with 100 contaminating *E. coli* reads, which should be, and is, closer to **ReadsOriginal** and **ReadsNew** than **ReadsMixed1**, with 2000 *E. coli* reads.

Figure 13 contains the ECDFs of Neighbor Similarity for all six datasets. That for **ReadsOriginal** (blue) is essentially completely overplotted by those for **ReadsNew** (cyan) and **ReadsMixed2** (green). Interestingly, but consistent with the Boundary columns in Table 8, **ReadsEcoli** is now the most different from **ReadsOriginal**, **ReadsNew** and **ReadsMixed2**, even though it contains “real” reads. We performed one- and two-sided Kolmogorov-Smirnov tests on selected pairs of the ECDFs in Figure 13. No difference involving **ReadsOriginal**, **ReadsNew** and **ReadsMixed2** was remotely significant. On the other hand, differences between **ReadsOriginal** and all of **ReadsMixed1**, **Random6K**, and **ReadsEcoli** were massively significant, in the latter two cases with  $p$ -values of zero.

---

<sup>10</sup>Contamination of DNA samples is a pervasive problem in multiple contexts, including analysis of ancient DNA (Reich, 2018).

The intriguing, to still-to-be-explored, implication is that the distributions of decisions, boundary status and Neighbor Similarity may be usable as diagnostics that indicate when the classifier is being used on data that differ from what was expected.

Table 9: Summary of results for the Bayes classifier applied to alternative datasets. Columns for Decision and Boundary are percentages.

Dataset	Count	Decision			Boundary	
		Adeno	COVID	SARS	No	Yes
ReadsOriginal	5869	32.94	34.09	32.97	69.48	30.52
ReadsNew	6000	32.43	33.82	33.75	68.7	31.3
ReadsMixed2	5969	33.86	33.59	32.55	69.69	30.31
ReadsMixed1	7869	48.1	26.2	25.7	74.1	25.9
ReadsEcoli	6000	92.767	2.933	4.300	87.35	12.65
Random6K	6000	90.8333	0.3833	8.7833	78.75	21.25

## 5 Conclusions

The two principal contributions of this paper are methods for investigating the boundary of classifiers and surrogate measures of uncertainty for classifiers without them.

In summary, we propose that Neighbor Similarity be used as a measure of uncertainty (or confidence) for classifiers lacking inherent measures of uncertainty, which may be in the majority among classifiers currently in use. Despite the computational burden, the potential to avoid incorrect decisions is enormous.

As always, at least as many questions are raised as were answered. Perhaps the most challenging is investigating whether Neighbor Similarity is viable in the context of production-grade classifiers such as SeqScreen. A—or perhaps even *the*—central issue may be whether the information gained justifies the computational cost. A DNA sequence of length 10,000 has more than 4 million neighbors, and running SeqScreen (or any other complex classifier) on all of them may be prohibitive. We showed the potential of sampling to estimate Neighbor Similarity from a subset of neighbors; devising demonstrably effective strategies to do so is a first priority.

Underlying everything is an issue—both scientific and statistical—that we have not addressed in this paper. When  $NS(R)$  is low, is it a statement about the read or about the classifier? This question needs more attention. As long there is a range of observed values of NS, and especially values near 1, then low values are plausibly statements about reads. On the other hand, uniformly small values of  $NS(R)$  seem suggestive of problems with the classifier. But then, what if the problem is just innately hard?

A classifier with a graph input space  $\mathcal{I}$  and discrete output space  $\mathcal{O}$  must have a boundary (actually, boundaries), and the evidence from our experiment is that  $\mathcal{B}$  is neither small nor thin. One final missing link is scientific insight into the boundary. In our setting, neighbors differ in exactly one nucleotide—and therefore at most one amino acid, the simplest of genetic mutations. Scientific scrutiny of boundary pairs could provide information about whether they really should be classified differently.

## Acknowledgements

This research was supported in part by NIH grant 5R01AI100947–06, “Algorithms and Software for the Assembly of Metagenomic Data,” to the University of Maryland College Park (Mihai Pop, PI). We thank Professor Pop for numerous insightful discussions.

## References

- Balaji, A., Kille, B., Kappell, A. D., Godbold, G. D., Diep, M., Elworth, R. A. L., Z., Albin, Q. D., Nasko, D. J., Shah, N., Pop, M., Segarra, S., Ternus, K. L., and Treangen, T. J. (2022). SeqScreen: accurate and sensitive functional screening of pathogenic sequences via ensemble learning. *Genome Biology*, 23:133.
- Breiman, L., Friedman, J., Olshen, R., and Stone, C. J. (2017). *Classification and Regression Trees*. CRC Press, Boca Raton, FL.
- Commichaux, S., Shah, N., Ghurye, J., Stoppel, A., Goodheart, J. A., Luque, G. G., Cummings, M. P., and Pop, M. (2021). A critical assessment of gene catalogs for metagenomic analysis. *Bioinformatics*. btab216.
- Diaconis, P. and Sturmfels, B. (1998). Algebraic algorithms for sampling from conditional distributions. *Ann. Statist.*, 26:363–97.
- Hastie, T., Tibshirani, R., and Friedman, J. (2001). *The Elements of Statistical Learning: Data Mining, Inference, and Prediction*. Springer–Verlag, New York.
- Holtgrewe, M. (2010). Mason: A read simulator for second generation sequencing data. *Technical Report FU Berlin*.
- Karr, A. F., Hauzel, J., Porter, A. A., and Schaefer, M. (2022a). Application of Markov structure of genomes to outlier identification and read classification. *BMC Bioinformatics*. Submitted for publication. arXiv:2112.13117.
- Karr, A. F., Hauzel, J., Porter, A. A., and Schaefer, M. (2022b). Measuring quality of DNA sequence data via degradation. *PLoS ONE*, 2022:0221459. DOI: 10.1371/journal.pone.0221459.
- Karr, A. F., Sanil, A. P., and Banks, D. L. (2006). Data quality: A statistical perspective. *Statistical Methodology*, 3(2):137–173.
- Langdon, W. B. (2014). Mycoplasma contamination in the 1000 genomes project. *BioData Mining*, 7:3.
- Navarro, G. (2001). A guided tour to approximate string matching. *ACM Computing Surveys*, 33(1):31–88.
- Nikulin, M. S. (2001). Hellinger distance. In *Encyclopedia of Mathematics*. EMS Press, Berlin.
- Pride, D. T., Meinersmann, R. J., Wassenaar, T. M., and Blaser, M. J. (2003). Evolutionary implications of microbial genome tetranucleotide frequency biases. *Genome Research*, 13:145–158.
- R Core Team (2020). *R: A Language and Environment for Statistical Computing*. R Foundation for Statistical Computing, Vienna, Austria.

- Reich, D. (2018). *Who We Are and How We Got Here: Ancient DNA and the New Science of the Human Past*. Vintage Books, New York.
- Steinegger, M. and Salzberg, S. L. (2020). Terminating contamination: large-scale search identifies more than 2,000,000 contaminated entries in GenBank. *Genome Biology*, 21(1):115.
- Teeling, H., Meyerdierks, A., Bauer, M., Amann, R., and Glöckner, F. O. (2004a). Application of tetranucleotide frequencies for the assignment of genomic fragments. *Environmental Microbiology*, 6(9):938–947.
- Teeling, H., Waldmann, J., Lombardot, T., Bauer, M., and Glöckner, F. O. (2004b). TETRA: a web-service and a stand-alone program for the analysis and comparison of tetranucleotide usage patterns in DNA sequences. *BMC Bioinformatics*, 5(163).
- Titterton, D., Smith, A., and Makov, U. (1985). *Statistical Analysis of Finite Mixture Distributions*. Wiley, New York.
- Wang, Q., Garrity, G. M., Tiedjel, J. M., and Cole, J. R. (2007). Naïve Bayesian classifier for rapid assignment of rRNA sequences into the new bacterial taxonomy. *Applied and Environmental Microbiology*, 73(16):5261–5267.

## A Triplet Distributions of the Three Genomes

Table 10: Triplet distributions for the adenovirus, COVID and SARS genomes used in this paper.

Triplet	Adeno	COVID	SARS	Triplet	Adeno	COVID	SARS
AAA	0.031826	0.026367	0.025581	GAA	0.017496	0.012899	0.015261
AAC	0.020016	0.010660	0.018051	GAC	0.012220	0.005982	0.012337
AAG	0.018463	0.016776	0.018891	GAG	0.013832	0.007252	0.013278
AAT	0.018551	0.030176	0.021917	GAT	0.011927	0.021621	0.015597
ACA	0.020016	0.012699	0.026219	GCA	0.017847	0.008221	0.014421
ACC	0.015327	0.006851	0.013076	GCC	0.015063	0.004278	0.007866
ACG	0.010316	0.003709	0.005210	GCG	0.015327	0.002373	0.004975
ACT	0.016265	0.016609	0.022018	GCT	0.016499	0.013868	0.020908
AGA	0.014213	0.016208	0.018085	GGA	0.016704	0.005514	0.011698
AGC	0.017701	0.007519	0.011765	GGC	0.014243	0.005247	0.009849
AGG	0.015591	0.008421	0.013984	GGG	0.012279	0.003409	0.004975
AGT	0.014711	0.019015	0.015059	GGT	0.013041	0.018346	0.013916
ATA	0.012836	0.024429	0.013345	GTA	0.013334	0.020151	0.014723
ATC	0.011224	0.010694	0.011294	GTC	0.010228	0.007419	0.009984
ATG	0.017378	0.029475	0.026085	GTG	0.014067	0.016308	0.018488
ATT	0.018990	0.038765	0.024438	GTT	0.016294	0.037562	0.019698
CAA	0.020573	0.012565	0.024471	TAA	0.018961	0.032148	0.019160
CAC	0.014008	0.006015	0.016202	TAC	0.015679	0.017244	0.019933
CAG	0.019342	0.008956	0.014891	TAG	0.010579	0.018179	0.011832
CAT	0.017115	0.012030	0.018589	TAT	0.012836	0.039533	0.019026
CCA	0.019400	0.006149	0.013311	TCA	0.013774	0.012498	0.020202
CCC	0.014067	0.002573	0.004773	TCC	0.013744	0.006115	0.007059
CCG	0.010257	0.001604	0.003059	TCG	0.008059	0.003676	0.005849
CCT	0.014506	0.009491	0.011631	TCT	0.014301	0.019416	0.019093
CGA	0.009055	0.002406	0.004672	TGA	0.015503	0.023593	0.022018
CGC	0.015503	0.001771	0.004471	TGC	0.017290	0.014203	0.022085
CGG	0.010257	0.001571	0.002756	TGG	0.018170	0.019115	0.018723
CGT	0.009143	0.005614	0.007194	TGT	0.017027	0.038464	0.026724
CTA	0.013012	0.017544	0.018723	TTA	0.018873	0.044981	0.023160
CTC	0.011459	0.007085	0.012000	TTC	0.016968	0.016508	0.018925
CTG	0.017525	0.014203	0.018891	TTG	0.019019	0.035390	0.026085
CTT	0.019576	0.020552	0.024034	TTT	0.030595	0.059985	0.027463

## B Details of Boundary Crawls

Here we given detailed results for the 100 boundary crawls. The variables in the tables are as follows:

**Length** is length of the crawl, which continues for either 250 steps or until it terminates at a “hair” of the boundary.

**Classifier Evaluations** is the number of sequences on which the classifier is run, which is 404 [neighbors per sequence]  $\times$  Length.

**N\_Adeno, N\_COVID, N\_SARS** are then numbers of sequences on the crawl classified as Adeno, COVID and SARS, respectively.

**N\_Decisions** is the number of genomes encounter on the path—either 2 or 3.

Table 11: Results for boundary crawls, part one.

Length	Classifier Evaluations	N_Adeno	N_COVID	N_SARS	N_Decisions
250	101000	125	0	125	2
250	101000	121	4	125	3
250	101000	117	9	124	3
250	101000	121	5	124	3
22	8888	2	9	11	3
250	101000	104	35	111	3
250	101000	99	37	114	3
242	97768	103	23	116	3
250	101000	92	41	117	3
250	101000	63	87	100	3
250	101000	125	0	125	2
40	16160	20	0	20	2
250	101000	125	0	125	2
151	61004	55	24	72	3
250	101000	125	0	125	2
250	101000	123	3	124	3
161	65044	68	30	63	3
250	101000	125	0	125	2
250	101000	122	18	110	3
103	41612	52	0	51	2
250	101000	113	20	117	3
250	101000	98	41	111	3
90	36360	42	7	41	3
146	58984	16	59	71	3
250	101000	110	41	99	3
206	83224	103	0	103	2
140	56560	19	52	69	3
250	101000	87	77	86	3
56	22624	11	18	27	3
5	2020	0	2	3	2
250	101000	120	13	117	3
250	101000	117	15	118	3
250	101000	125	0	125	2
130	52520	65	0	65	2
220	88880	110	0	110	2
250	101000	125	0	125	2
250	101000	125	0	125	2
250	101000	83	50	117	3
250	101000	125	0	125	2
250	101000	98	29	123	3
139	56156	35	35	69	3
250	101000	104	35	111	3
250	101000	113	13	124	3
250	101000	125	0	125	2
152	61408	35	49	68	3
235	94940	74	65	96	3
35	14140	17	0	18	2
250	101000	110	17	123	3
250	101000	121	9	120	3
250	101000	125	0	125	2

Table 12: Results for boundary crawls, part one.

Length	Classifier Evaluations	N_Adeno	N_COVID	N_SARS	N_Decisions
250	101000	108	19	123	3
94	37976	47	0	47	2
250	101000	106	28	116	3
250	101000	95	62	93	3
250	101000	125	0	125	2
103	41612	52	0	51	2
220	88880	110	0	110	2
141	56964	71	0	70	2
130	52520	57	21	52	3
250	101000	113	18	119	3
135	54540	68	0	67	2
250	101000	125	0	125	2
117	47268	59	0	58	2
250	101000	104	23	123	3
250	101000	125	0	125	2
41	16564	2	19	20	3
227	91708	64	59	104	3
250	101000	111	15	124	3
250	101000	71	114	65	3
250	101000	110	22	118	3
76	30704	38	0	38	2
250	101000	110	60	80	3
22	8888	0	11	11	2
250	101000	111	21	118	3
73	29492	37	0	36	2
250	101000	108	26	116	3
250	101000	116	17	117	3
150	60600	32	50	68	3
34	13736	17	0	17	2
250	101000	125	0	125	2
250	101000	125	0	125	2
250	101000	125	0	125	2
69	27876	24	13	32	3
250	101000	124	12	114	3
250	101000	118	39	93	3
250	101000	113	34	103	3
250	101000	125	0	125	2
250	101000	124	2	124	3
53	21412	27	0	26	2
250	101000	109	23	118	3
13	5252	7	0	6	2
250	101000	125	0	125	2
250	101000	77	51	122	3
250	101000	125	0	125	2
250	101000	125	0	125	2
193	77972	76	21	96	3
250	101000	93	40	117	3
250	101000	123	2	125	3
250	101000	125	0	125	2
250	101000	125	0	125	2

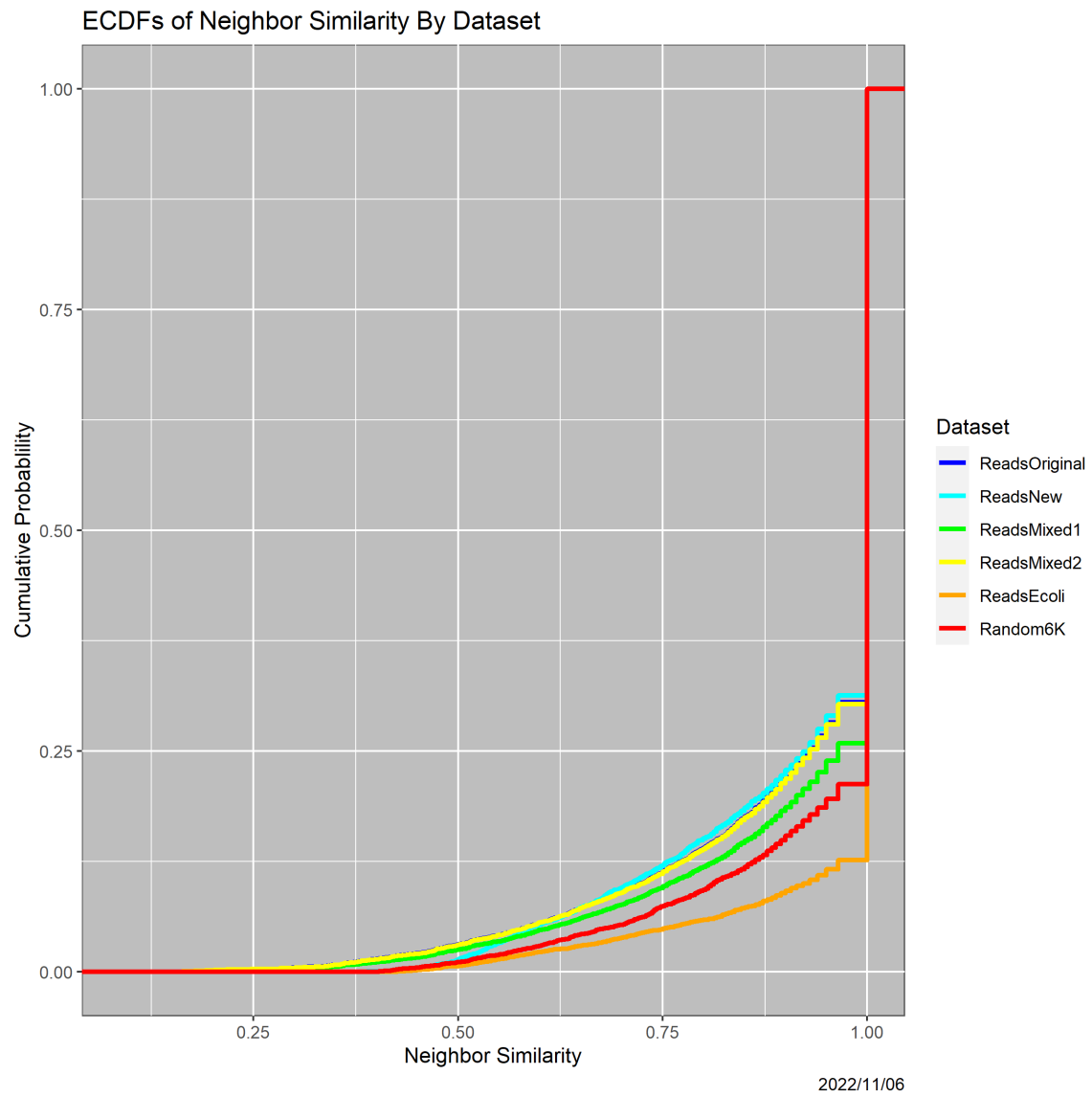


Figure 13: